
Factorization-Error-Free Discrete Diffusion Language Model via Speculative Decoding

Xun Fang

East China Normal University
51264404020@stu.ecnu.edu.cn

Yunchen Li

East China Normal University
52284404001@stu.ecnu.edu.cn

Hang Yuan

East China Normal University
Beijing Zhongguancun Academy
52274404018@stu.ecnu.edu.cn

Zhou Yu*

East China Normal University
zyu@stat.ecnu.edu.cn

Abstract

Discrete diffusion language models improve generation efficiency through parallel token prediction, but standard X_0 prediction methods introduce factorization errors by approximating the clean token posterior with independent token-wise distributions. This paper proposes Factorization-Error-Free Discrete Diffusion Language Modeling (FeF-DLLM), which replaces independent clean-token prediction with an exact prefix-conditioned factorization of the clean posterior to better preserve token dependencies. To reduce the sequential cost introduced by prefix conditioning, FeF-DLLM further incorporates speculative decoding within diffusion denoising, accelerating inference while maintaining the parallel prediction and re-masking properties of DLLMs. Theoretically, we prove that FeF-DLLM generates from the true joint distribution and derive its expected acceleration ratio. Experiments on GSM8K, MATH, HumanEval, and MBPP demonstrate that our method improves accuracy by an average of 5.04 percentage points while achieving an average inference speedup of $3.86\times$.

1 Introduction

Diffusion models [Ho et al., 2020, Lipman et al., 2022, Song et al., 2020b,a] have become one of the most successful classes of generative models in recent years, achieving strong performance in image generation [Rombach et al., 2022, Peebles and Xie, 2023, Ma et al., 2024], video generation [Ho et al., 2022, Bar-Tal et al., 2024], and many other domains [Wu et al., 2024, Yim et al., 2024, Wang et al., 2025]. Recently, several works have extended diffusion modeling to discrete spaces [Austin et al., 2021a, Lou et al., 2024, Gat et al., 2024, Sahoo et al., 2024] and applied discrete diffusion language models (DLLMs) to large language modeling [Nie et al., 2025, Ye et al., 2025, Bie et al., 2025]. These models have shown competitive performance with autoregressive models while enabling a different generation paradigm based on iterative denoising and parallel token prediction.

During generation, DLLMs usually predict multiple tokens in parallel and combine these token-wise predictions to form the final output. Although this design improves generation efficiency, it introduces a factorization error because the joint distribution over clean tokens is approximated by a product of independent token distributions. Recent works have attempted to address this issue from different perspectives. ReDi [Yoo et al., 2025] mitigates factorization error through a rectified-flow formulation

The authors contribute equally to the paper and are listed in alphabetical order.

*Corresponding author.

and newly constructed paired training data, but it does not fully remove the error. Other methods propose improved sampling procedures [Liu et al., 2024, Lavenant and Zanella, 2025], often at the cost of significantly slower generation. Some approaches integrate DLLMs with speculative decoding [Campbell et al., 2025, Cheng et al., 2025]; however, such designs introduce autoregressive decoding behavior into DLLM inference, thereby undermining the distinctive non-autoregressive reasoning characteristics of DLLMs.

In this paper, we propose *Factorization-Error-Free Discrete Diffusion Language Modeling* (FeF-DLLM). Built upon the classical X_0 -prediction framework of DLLMs, FeF-DLLM analyzes the exact decomposition of the clean posterior distribution and derives a factorization-error-free generation objective. Instead of independently predicting each clean token, our method uses prefix-conditioned prediction to preserve dependencies among clean tokens. To improve inference efficiency, we further incorporate speculative decoding, which amortizes the sequential dependency introduced by prefix conditioning and accelerates generation while retaining the parallel prediction and re-masking properties of DLLMs.

We theoretically show that FeF-DLLM can generate samples from the true conditional joint distribution when the position-conditioned target model is well specified, and we analyze the expected speedup brought by speculative decoding. We evaluate FeF-DLLM on standard mathematical reasoning and code generation benchmarks, including GSM8K, MATH, HumanEval, and MBPP. Experimental results show that FeF-DLLM improves accuracy by an average of 5.04 percentage points and achieves an average inference speedup of $3.86\times$, demonstrating its effectiveness in improving generation quality while substantially accelerating inference.

Our contributions are summarized as follows:

- We analyze the factorization error in existing DLLMs and show that it can be eliminated through an exact prefix-conditioned factorization of the clean posterior.
- We use speculative decoding to accelerate the resulting prefix-conditioned inference procedure and derive its expected speedup.
- We conduct extensive experiments to evaluate FeF-DLLM. Experimental results demonstrate that FeF-DLLM consistently improves generation quality over the baseline while simultaneously achieving substantial wall-clock acceleration.

2 Preliminary

2.1 Discrete Diffusion Language Models

Discrete diffusion language models define a diffusion process directly over discrete tokens. Building on the D3PM framework [Austin et al., 2021a], we define the forward diffusion process as a fixed Markov chain $q(X_{1:T} | X_0) = \prod_{t=1}^T q(X_t | X_{t-1})$, in which each transition kernel is parameterized by a categorical transition matrix $Q_t \in \mathbb{R}^{S \times S}$, where S denotes the vocabulary size. For a one-hot token X_{t-1} , the one-step corruption process is

$$q(X_t | X_{t-1}) = \text{Cat}(X_t; p = X_{t-1}Q_t),$$

where $\text{Cat}(x; p)$ denotes a categorical distribution over the one-hot row vector x , with probabilities given by row vector p . Let $\bar{Q}_t = Q_1 Q_2 \cdots Q_t$. The marginal at timestep t is $q(X_t | X_0) = \text{Cat}(X_t; p = X_0 \bar{Q}_t)$, enabling noisy tokens to be sampled directly from the clean input. For sequence data, corruption is typically applied independently across token positions. Common choices of Q_t include uniform transitions, nearest-neighbor transitions in embedding space, and absorbing-state transitions that gradually replace tokens with a special [MASK] token.

The forward posterior has the following closed form:

$$q(X_{t-1} | X_t, X_0) = \text{Cat} \left(X_{t-1}; p = \frac{X_t Q_t^\top \odot X_0 \bar{Q}_{t-1}}{X_0 \bar{Q}_t X_t^\top} \right).$$

The generative process is a learned reverse Markov chain $p_\theta(X_{0:T}) = p(X_T) \prod_{t=1}^T p_\theta(X_{t-1} | X_t)$. In the X_0 -prediction parameterization, the model first predicts the clean token from the corrupted

input, denoted as $\hat{X}_0 = f_\theta(X_t, t)$. Then the reverse transition is constructed by plugging this prediction into the analytic forward posterior:

$$p_\theta(X_{t-1} | X_t) = q(X_{t-1} | X_t, \hat{X}_0). \quad (1)$$

Equivalently, the model uses the predicted clean token to determine how to denoise X_t by one step. The corresponding clean-token prediction objective is

$$\mathcal{L} = \mathbb{E}_{q(X_0)} \mathbb{E}_t \mathbb{E}_{q(X_t | X_0)} \left[- \sum_{i=1}^N \log p_\theta(X_0^i | X_t, t) \right]. \quad (2)$$

2.2 Speculative Decoding

Speculative decoding [Leviathan et al., 2023, Chen et al., 2023] accelerates autoregressive inference by using a smaller and faster approximation model to propose multiple candidate tokens, which are then verified in parallel by the target model. Let M_π denote the target model, and let $\pi(X^i | X^{<i})$ be its next-token distribution given the prefix $X^{<i}$. We further introduce an efficient approximation model M_ρ , whose next-token distribution is denoted by $\rho(X_t | X^{<i})$. Speculative decoding proceeds as follows. First, the approximation model M_ρ autoregressively generates γ candidate tokens, denoted by X^1, \dots, X^γ . Then, the target model M_π evaluates the corresponding candidate prefixes in parallel and obtains the target distributions at each position. For the i -th proposed token X^i , the algorithm accepts it with probability

$$\min \left(1, \frac{\pi_i(X^i)}{\rho_i(X^i)} \right),$$

where π_i and ρ_i denote the target and approximation distributions under the corresponding prefix, respectively. If a proposed token is rejected, the algorithm resamples from the corrected distribution

$$\pi'(X) = \text{norm}(\max(0, \pi(X) - \rho(X))).$$

This correction ensures that the resulting sample is still exactly distributed according to the target distribution π . Therefore, speculative decoding produces samples from the same distribution as direct decoding from M_π . Benefiting from the parallel verification of multiple draft tokens, speculative decoding can substantially improve generation speed.

2.3 Setting and Notation

We consider a d -dimensional discrete random variable $X = (X^1, \dots, X^d)^\top$ defined on \mathcal{V}^d . Subscripts are used to index decoding steps in diffusion language model inference, while superscripts are used to index token positions in a sequence. For example, X_t^i denotes the random token at position i when the diffusion decoder is at step t . We write $X^{<i}$ and $X^{>i}$ to denote the subsequence of tokens before and after position i . In the context of speculative decoding, we use π to denote the target distribution and ρ to denote the draft distribution. \odot is denoted as element-wise multiplication.

3 Methodology

3.1 Analysis of Factorization Error

We first revisit the commonly used X_0 -prediction parameterization in discrete diffusion language models. Given a corrupted sequence X_t , the reverse transition in Eq. 1 is constructed from an estimate of the clean-data posterior $p(X_0 | X_t)$. In principle, this posterior is a distribution over the full discrete sequence space \mathcal{V}^d , whose cardinality grows exponentially with the sequence length d . Directly modeling such a joint distribution is computationally intractable for neural language models. Therefore, existing DLLMs usually adopt a token-wise prediction objective, in which the model predicts each clean token independently conditioned on the same corrupted input:

$$p(X_0 | X_t) \approx \prod_{i=1}^d p(X_0^i | X_t). \quad (3)$$

However, Eq. 3 relies on an independence assumption across dimensions. Such an assumption is generally incompatible with natural language, where tokens exhibit strong syntactic and semantic dependencies. The exact decomposition of the clean posterior follows the chain rule:

$$p(X_0 | X_t) = \prod_{i=1}^d p(X_0^i | X_t, X_0^{<i}).$$

Compared with Eq. 3, this factorization preserves dependencies among clean tokens by conditioning each position on the previously recovered clean prefix $X_0^{<i}$. The discrepancy between the token-wise approximation and the exact factorization is therefore characterized by the missing dependence on $X_0^{<i}$. To make this discrepancy explicit, we derive the following identity.

Lemma 1. *Assume that the forward corruption process factorizes across token positions, i.e., $q(X_t | X_0) = \prod_{j=1}^d q(X_t^j | X_0^j)$. For any position i , the autoregressive clean-token posterior satisfies*

$$\begin{aligned} p(X_0^i | X_t, X_0^{<i}) &= p(X_0^i | X_t^{\geq i}, X_0^{<i}) \\ &\propto p(X_0^i | X_t) \frac{p(X_0^i | X_t^{\geq i}, X_0^{<i})}{p(X_0^i | X_t^{-i})}, \end{aligned}$$

where $X_t^{-i} = (X_t^{<i}, X_t^{\geq i})$, and the proportionality is over X_0^i .

Lemma 1 shows that the desired autoregressive posterior $p(X_0^i | X_t, X_0^{<i})$ is equivalent to conditioning on $(X_t^{\geq i}, X_0^{<i})$, and differs from the independent predictor $p(X_0^i | X_t)$ by the normalized correction term $p(X_0^i | X_t^{\geq i}, X_0^{<i})/p(X_0^i | X_t^{-i})$. This term captures the additional dependence on the clean prefix and the remaining corrupted context. Therefore, predicting the i -th clean token should account not only for the corrupted sequence X_t , but also for previously determined clean tokens; ignoring this dependence leads to factorization error in the learned reverse process.

Motivated by this observation, we replace the independent clean-token predictor with a prefix-conditioned predictor. Instead of estimating $p_\theta(X_0^i | X_t, t)$ independently for each position, we train the model to approximate

$$p_\theta(X_0^i | X_t^{\geq i}, X_0^{<i}, t).$$

This parameterization preserves the left-to-right dependency structure of the clean sequence while still leveraging the bidirectional corrupted context available in diffusion inference. The resulting training objective is

$$\mathcal{L} = \mathbb{E}_{q(X_0)} \mathbb{E}_t \mathbb{E}_{q(X_t | X_0)} \left[- \sum_{i=1}^d \log p_\theta(X_0^i | X_t^{\geq i}, X_0^{<i}, t) \right]. \quad (4)$$

This objective has the same supervised clean-token prediction form as Eq. 2. Consequently, it can be optimized by finetuning existing DLLM backbones with modified input, without changing the underlying discrete diffusion forward process. The corresponding training procedure is summarized in Algorithm 1 in Appendix C.

3.2 Acceleration via Speculative Decoding

The prefix-conditioned predictor introduced in Eq. 4 enables inference from the correct joint distribution of clean tokens, thereby eliminating the factorization error induced by the independence assumption, but it also changes the inference pattern of DLLMs. In standard DLLM inference, all clean-token predictions can be produced in parallel from the corrupted sequence X_t . In contrast, $p_\theta(X_0^i | X_t^{\geq i}, X_0^{<i}, t)$ depends on the previously recovered clean prefix $X_0^{<i}$. Therefore, directly sampling from this distribution requires left-to-right decoding within each denoising step, which may reduce the parallel efficiency of diffusion-based generation.

To mitigate this sequential bottleneck, we adopt speculative decoding within each diffusion denoising step. The key idea is to use a fast draft model to propose multiple clean tokens in parallel, and then verify these proposals with the prefix-conditioned target model. The complete inference algorithm is provided in Algorithm 2 in Appendix C. Suppose that the first m positions have already been

determined, denoted by $\hat{X}_0^{<m}$. We consider a speculative window of length k , covering positions $m+1, \dots, m+k$. The draft model defines a distribution

$$\rho_\phi^i(X_0^i) := \rho_\phi(X_0^i | \hat{X}_0^{<m}, X_t^{>m}, t), \quad i = m+1, \dots, m+k.$$

Unlike the target model, the draft model conditions only on the already verified prefix $\hat{X}_0^{<m}$ and the remaining corrupted context $X_t^{>m}$. Thus, the draft distributions for all positions in the speculative window can be computed in parallel. We then sample draft tokens $\tilde{X}_0^{m+1}, \dots, \tilde{X}_0^{m+k} \sim \prod_{i=m+1}^{m+k} \rho_\phi^i(\cdot)$. After the draft tokens are generated, the target model verifies them from left to right. For each position $i = m+1, \dots, m+k$, the target distribution is evaluated using the prefix formed by the already accepted tokens and the preceding draft tokens:

$$\pi_\theta^i(X_0^i) := p_\theta(X_0^i | X_t^{\geq i}, \tilde{X}_0^{<i}, t).$$

The proposed token \tilde{X}_0^i is accepted with probability

$$\min\left(1, \frac{\pi_\theta^i(\tilde{X}_0^i)}{\rho_\phi^i(\tilde{X}_0^i)}\right).$$

If \tilde{X}_0^i is accepted, we set $\hat{X}_0^i = \tilde{X}_0^i$ and continue to verify the next position. If it is rejected, we resample \hat{X}_0^i from the corrected distribution

$$\pi_\theta^i(x) = \text{norm}\left(\max(0, \pi_\theta^i(x) - \rho_\phi^i(x))\right),$$

and terminate the current speculative window. The next speculative step then starts from the updated verified prefix. This procedure is repeated until all positions in the block have been inferred, yielding a complete prediction \hat{X}_0 . Once \hat{X}_0 is obtained, we construct the reverse transition following the standard X_0 -prediction parameterization:

$$p_\theta(X_{t-1} | X_t) = q(X_{t-1} | X_t, \hat{X}_0),$$

as in Eq. 1. Therefore, our method modifies only the clean-token prediction stage, while leaving the discrete forward process and the analytic posterior transition unchanged.

The choice of the draft model is flexible. In principle, any model that approximates the target conditional distribution and supports efficient sampling can be used as ρ_ϕ . In practice, we use a DLLM-style draft model because its token predictions can be computed in parallel within a speculative window, resulting in an $O(1)$ drafting cost with respect to the window length. Moreover, using a draft model with the same architecture family as the target model often yields higher acceptance rates, since the draft distribution is better aligned with the prefix-conditioned target distribution. The complete inference algorithm is provided in Algorithm 2 in Appendix C. The overall training and inference pipeline of FeF-DLLM is illustrated in Figure 1.

3.3 Theoretical Properties

We establish two theoretical properties of FeF-DLLM. The first result shows that the proposed prefix-conditioned generation rule is distributionally exact whenever the target model matches the true position-conditioned posterior. The second result characterizes the expected progress of speculative verification under a standard independent-acceptance approximation.

Distributional exactness. Fix a denoising state X_t and let

$$J_t = \{j_1, \dots, j_{L_t}\}, \quad j_1 < \dots < j_{L_t},$$

be the ordered set of positions to be updated at timestep t . Let p^* denote the oracle data law. We assume the target law π_θ induced by p_θ matches the true position-conditioned posterior under p^* . For every $m \in \{1, \dots, L_t\}$, we take the target model to be the oracle next-position law

$$\pi_\theta^{j_m}(x) = p^*\left(X_0^{j_m} = x \mid X_t^{\geq j_m}, X_0^{<j_m}, t\right). \quad (5)$$

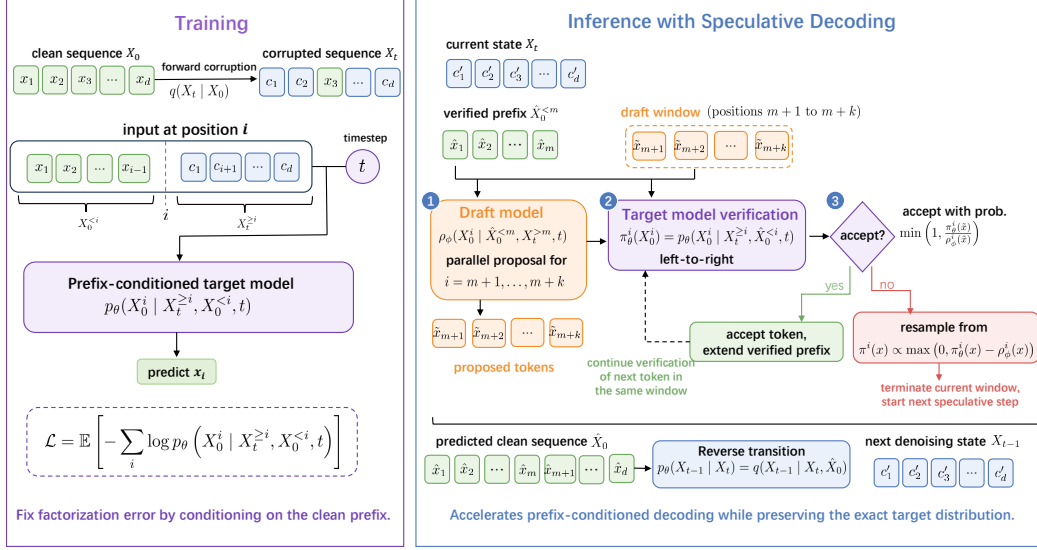


Figure 1: Overview of FeF-DLLM. Prefix-conditioned training predicts each clean token from the clean prefix $X_0^{<i}$ and the remaining corrupted context $X_t^{>i}$. During inference, a draft model proposes a speculative window in parallel, and a prefix-conditioned target model verifies the proposals left to right before constructing the standard reverse transition.

Theorem 1 (Exact joint law). *Under Eq. 5, the sequence produced by FeF-DLLM satisfies, for any $x_{J_t} \in \mathcal{V}^{L_t}$,*

$$\Pr\left(\hat{X}_{0,J_t} = x_{J_t} \mid X_t, t\right) = \prod_{m=1}^{L_t} p^*\left(X_0^{j_m} = x^{j_m} \mid X_t^{\geq j_m}, x_0^{<j_m}, t\right).$$

Equivalently,

$$\Pr\left(\hat{X}_{0,J_t} = x_{J_t} \mid X_t, t\right) = p^*(x_{J_t} \mid X_t, t).$$

Corollary 1 (Conditional correctness under resampling). *Consider any resampling pass $s \geq 1$, and let*

$$R^{(s)} = \{r_1^{(s)}, \dots, r_{L_s}^{(s)}\}, \quad r_1^{(s)} < \dots < r_{L_s}^{(s)},$$

be the positions selected for resampling. Conditional on the previous sequence $\hat{X}_0^{(s-1)}$ and the selected set $R^{(s)}$, assume Eq. 5 holds on $R^{(s)}$, then for any $x_{R^{(s)}} \in \mathcal{V}^{L_s}$,

$$\Pr\left(\hat{X}_{0,R^{(s)}}^{(s)} = x_{R^{(s)}} \mid \hat{X}_0^{(s-1)}, R^{(s)}, t\right) = p^*\left(x_{R^{(s)}} \mid \hat{X}_0^{(s-1)}, R^{(s)}, t\right).$$

The corollary is a conditional statement: once the resampling set is fixed, the same distributional correctness argument applies to the selected positions. Therefore, repeated low-confidence resampling preserves the correctness of each conditional regeneration step.

Expected speculative progress. We next quantify the expected number of positions committed in one speculative round. Let k denote the window size and let α denote the average probability that a draft token is accepted by the target model. Following the standard analysis of speculative decoding [Leviathan et al., 2023], we assume that acceptance events within a window are independent.

Theorem 2 (Expected committed length). *Let C_k be the number of positions committed in one speculative round, where the first rejected position, if any, is also committed after correction. Then*

$$\mathbb{E}[C_k] = \sum_{\ell=0}^{k-1} \alpha^\ell = \begin{cases} \frac{1 - \alpha^k}{1 - \alpha}, & 0 \leq \alpha < 1, \\ k, & \alpha = 1. \end{cases}$$

Corollary 2 (Idealized acceleration ratio). *Let c_ρ and c_π denote the wall-clock costs of one draft proposal pass and one target verification pass, respectively. Relative to a prefix-conditioned sequential target baseline that commits one position per target pass, the idealized expected acceleration ratio is*

$$S = \frac{\mathbb{E}[C_k] c_\pi}{c_\rho + c_\pi}.$$

In particular, if $c_\rho \approx c_\pi$, then

$$S \approx \frac{\mathbb{E}[C_k]}{2} = \begin{cases} \frac{1 - \alpha^k}{2(1 - \alpha)}, & 0 \leq \alpha < 1, \\ \frac{k}{2}, & \alpha = 1. \end{cases}$$

Thus, larger windows and higher acceptance rates increase the expected number of committed positions per speculative round, while the actual wall-clock gain is additionally modulated by the relative costs of drafting and verification.

4 Experiment

4.1 Experimental Setup

We use a supervised finetuning set of 72 thousand prompt–response pairs for training, covering both code and math data. Each training example is organized as a prompt–response pair, where only response tokens are masked and predicted. The finetuned base model is optimized with the proposed position-conditioned objective in Eq. 4. We optimize all models with AdamW using a weight decay of 0.1. The learning rate is initialized at 1×10^{-5} , with 50 warmup steps, followed by a constant phase and a linear decay over the final 10% of training steps to 0.1 times the peak learning rate. We use a per-device batch size of 1 and gradient accumulation over 2 steps, yielding a global batch size of 16. We train for 1 epochs and use bf16 mixed precision.

During speculation, both the draft and target models in speculative decoding are instantiated with the fine-tuned model, and the window size is set to 16. This choice is further validated in the ablation study. All training and inference experiments are conducted on 8 NVIDIA A100 80GB GPUs.

4.2 Main Results

We evaluate the models on four widely used benchmarks: GSM8K [Cobbe et al., 2021], MATH [Hendrycks et al., 2021], HumanEval [Chen et al., 2021], and MBPP [Austin et al., 2021b], covering both mathematical reasoning and code generation. To ensure reproducibility, we rely on the standardized OpenCompass [Contributors, 2023] evaluation pipeline. We report two main metrics: Accuracy, which measures final task performance, and Speedup, which measures the wall-clock acceleration ratio relative to the baseline decoding method. In all experiments, we use the inference time of LLaDA-Instruct as the reference runtime, denoted as $1 \times$.

We adopt LLaDA-Instruct [Nie et al., 2025] as the backbone model and build our method upon it; consequently, LLaDA-Instruct serves as the primary baseline for comparison. In addition, we compare our approach with several representative methods, including SSD [Gao et al., 2025], DDOSP [Lavenant and Zanella, 2025], and DCD [Liu et al., 2024]. Since the original papers, with the exception of LLaDA-Instruct, do not report results on the benchmarks considered in this work, we reproduce all remaining baselines under a unified evaluation protocol. Further implementation details are provided in Appendix A. It is worth noting that the original LLaDA decodes only one token at

Table 1: Main results on mathematical reasoning and code generation benchmarks. Best accuracy values are in bold, and fastest speed values are underlined. Mean denotes the average results across all four benchmarks. For FeF-DLLM, step denotes the number of diffusion model steps.

Methods	GSM8K		MATH		HumanEval		MBPP		Mean	
	Acc.	Speed	Acc.	Speed	Acc.	Speed	Acc.	Speed	Acc.	Speed
LLaDA [Nie et al., 2025]	78.60	1.00×	26.60	1.00×	47.60	1.00×	34.20	1.00×	46.75	1.00×
LLaDA/2 [Nie et al., 2025]	76.42	1.92×	25.46	1.99×	32.32	2.02×	35.00	1.98×	42.30	1.98×
SSD [Gao et al., 2025]	77.10	2.23×	34.94	2.16×	43.09	2.12×	39.20	1.83×	48.58	2.09×
DDOSP [Lavenant and Zanella, 2025]	74.15	1.92×	25.78	2.03×	28.05	2.01×	29.20	1.98×	39.30	1.98×
DCD [Liu et al., 2024]	78.24	0.36×	26.36	0.51×	50.00	0.43×	37.60	0.40×	48.05	0.43×
FeF-DLLM (step=2)	79.38	3.55×	36.40	3.25×	48.78	3.76×	42.60	4.89×	51.79	3.86×
FeF-DLLM (step=4)	79.68	2.14×	36.56	1.99×	49.39	2.21×	42.60	2.99×	52.06	2.33×

each step, which partially mitigates factorization error. To more directly evaluate the effectiveness of our method under a comparable multi-token decoding setting, we additionally reproduce a variant of LLaDA that decodes two tokens per step, denoted as LLaDA/2. The results are reported in Table 1.

We draw two key observations from Table 1. First, increasing the number of tokens decoded at each step can substantially improve inference throughput, but it may also lead to a pronounced degradation in generation quality. For example, LLaDA/2 achieves approximately a 2× speedup over LLaDA; however, its performance decreases on GSM8K, MATH, and HumanEval. This suggests that simply increasing decoding parallelism, in the absence of an explicit correction mechanism, can exacerbate factorization errors and compromise prediction accuracy. This observation validates our motivation that efficient parallel decoding for diffusion language models requires an effective correction mechanism to mitigate factorization errors.

Second, FeF-DLLM provides a stronger accuracy–efficiency trade-off than the baseline, direct speculative decoding methods, and prior approaches for mitigating factorization errors. Averaged over the four benchmarks, FeF-DLLM with step=2 improves the mean accuracy from 46.75 to 51.79, achieving a 5.04 point gain over LLaDA, while boosting the mean decoding speed to 3.86×. When using step=4, FeF-DLLM further increases the mean accuracy to 52.06, yielding a 5.31 point improvement over LLaDA, while still providing a 2.33× speedup. Notably, FeF-DLLM also surpasses SSD, a direct speculative decoding baseline, by 3.21 and 3.48 accuracy points under step=2 and step=4, respectively. In addition, compared with factorization-error mitigation methods such as DDOSP and DCD, FeF-DLLM achieves substantially faster inference, showing that resampling-based correction can effectively improve accuracy while preserving high decoding efficiency.

4.3 Ablation Study

We conduct four ablation studies to evaluate the contributions of different components in FeF-DLLM, focusing on the effects of training, speculative decoding, draft-model selection and window size of speculative decoding.

Ablation 1: Training Effects LLaDA-Instruct can also be directly used for inference with the proposed method without further finetuning its neural network parameters. Meanwhile, to rule out the possibility that the observed improvements are primarily attributable to finetuning rather than to the proposed inference strategy, we also evaluate the trained model using the original inference procedure of LLaDA-Instruct. The results are reported in Table 2.

The trained LLaDA model exhibits slight performance drops on GSM8K, MATH, and HumanEval, and only improves on MBPP. In contrast, FeF-DLLM with training consistently outperforms its untrained counterpart across all four benchmarks. These results demonstrate that the gains achieved by our method are driven by the joint effect of finetuning and the proposed inference strategy.

Ablation 2: Effect of Speculative Decoding To demonstrate the acceleration effect of speculative decoding, we compare FeF-DLLM with a counterpart that uses the same model but disables speculative decoding. Table 3 reports the results. Here, FeF-DLLM w/o SD denotes the non-speculative

The reproduced LLaDA accuracy on MBPP is 37.40; we report 34.20 from the original LLaDA result for consistency.

Table 2: Ablation study on training effects. Best accuracy values within each comparison group are in bold. Mean denotes the average results across all four benchmarks.

Methods	GSM8K		MATH		HumanEval		MBPP		Mean	
	Acc.	Speed	Acc.	Speed	Acc.	Speed	Acc.	Speed	Acc.	Speed
LLaDA	78.60	1.00×	26.60	1.00×	47.60	1.00×	34.20	1.00×	46.75	1.00×
LLaDA w/ train	76.19	1.00×	26.38	1.00×	46.34	1.00×	36.20	1.00×	46.28	1.00×
FeF-DLLM w/o train (step=2)	77.86	3.59×	35.20	3.30×	46.95	3.88×	40.60	4.92×	50.15	3.92×
FeF-DLLM w/o train (step=4)	77.86	2.17×	35.48	2.01×	47.56	2.29×	40.40	3.01×	50.33	2.37×
FeF-DLLM (step=2)	79.38	3.55×	36.40	3.25×	48.78	3.76×	42.60	4.89×	51.79	3.86×
FeF-DLLM (step=4)	79.68	2.14×	36.56	1.99×	49.39	2.21×	42.60	2.99×	52.06	2.33×

Table 3: Ablation study on the effect of speculative decoding (SD). All models in this table are trained models. Mean denotes the average results across all four benchmarks.

Methods	GSM8K		MATH		HumanEval		MBPP		Mean	
	Acc.	Speed	Acc.	Speed	Acc.	Speed	Acc.	Speed	Acc.	Speed
FeF-DLLM w/o SD (step=2)	79.38	0.69×	36.40	0.67×	48.78	0.66×	42.60	0.67×	51.79	0.67×
FeF-DLLM w/o SD (step=4)	79.68	0.41×	36.56	0.40×	49.39	0.39×	42.60	0.40×	52.06	0.40×
FeF-DLLM (step=2)	79.38	3.55×	36.40	3.25×	48.78	3.76×	42.60	4.89×	51.79	3.86×
FeF-DLLM (step=4)	79.68	2.14×	36.56	1.99×	49.39	2.21×	42.60	2.99×	52.06	2.33×

setting. The results show that incorporating speculative decoding substantially improves inference speed while preserving accuracy.

Ablation 3: Choice of Draft Model In all previous experiments, we use the same model as both the draft model and the verify model by default. Here, we further analyze how the choices of draft models affect final performance. The results are reported in Table 4. In addition to task accuracy and wall-clock speedup, we also report the average Acceptance, which measures the fraction of draft tokens accepted by the verify model.

The results show that the final accuracy remains unchanged across the two draft-model choices on all four benchmarks. This suggests that, in this setting, the verify model primarily determines the final prediction quality. Meanwhile, using the same model for both drafting and verification leads to consistently higher acceptance rates and slightly better speedup. This observation is consistent with our analysis in Corollary 2: when the draft model and the verify model are better aligned, the verify model accepts more draft tokens, which leads to more efficient speculative decoding.

Ablation 4: Speculative Decoding Window Size We further study the effect of the speculative decoding window size. Table 5 reports the results with resampling step = 4. The results show that increasing the window size substantially improves decoding speed while preserving the same accuracy. Larger window sizes could not be implemented due to device limitations. Therefore, a window size of 16 was selected for the formal experiment.

5 Limitation and Conclusion

In this paper, we proposed FeF-DLLM, a factorization-error-free discrete diffusion language modeling method based on prefix-conditioned clean-token prediction. By replacing independent token-wise prediction with exact prefix-conditioned factorization, FeF-DLLM preserves token dependencies and eliminates factorization error. We further incorporated speculative decoding to accelerate inference while maintaining the correctness of the target distribution. Experiments on mathematical reasoning and code generation benchmarks show that FeF-DLLM improves generation quality and achieves substantial inference speedup.

One limitation of our method is that prefix-conditioned prediction and speculative verification require more computational resources during inference than standard DLLM decoding. Future work will explore more resource-efficient implementations to further reduce this overhead.

Table 4: Ablation study on the choice of draft models. “A / B” denotes using A as the draft model and B as the verify model. All results are reported with resampling step = 4.

Task	FeF-DLLM / FeF-DLLM			FeF-DLLM w/o train / FeF-DLLM		
	Acc.	Speed	Acceptance	Acc.	Speed	Acceptance
GSM8K	79.68	2.14×	63.29	79.68	2.12×	62.55
MATH	36.56	1.99×	58.24	36.56	1.93×	56.17
HumanEval	49.39	2.21×	65.99	49.39	2.17×	64.52
MBPP	42.60	2.99×	92.84	42.60	2.89×	91.77

Table 5: Ablation study on the speculative decoding window size. All results are reported with resampling step = 4. Mean denotes the average results across all four benchmarks.

Variant	Window Size	GSM8K		MATH		HumanEval		MBPP		Mean	
		Acc.	Speed	Acc.	Speed	Acc.	Speed	Acc.	Speed	Acc.	Speed
FeF-DLLM	4	79.68	0.77×	36.56	0.76×	49.39	0.77×	42.60	0.80×	52.06	0.78×
	8	79.68	1.38×	36.56	1.34×	49.39	1.40×	42.60	1.57×	52.06	1.42×
	16	79.68	2.14×	36.56	1.99×	49.39	2.21×	42.60	2.99×	52.06	2.33×

References

- Jacob Austin, Daniel D. Johnson, Jonathan Ho, Daniel Tarlow, and Rianne Van Den Berg. Structured denoising diffusion models in discrete state-spaces. In *Advances in Neural Information Processing Systems (NeurIPS)*, volume 34, pages 17981–17993, 2021a.
- Jacob Austin, Augustus Odena, Maxwell Nye, Maarten Bosma, Henryk Michalewski, David Dohan, Ellen Jiang, Carrie Cai, Michael Terry, Quoc Le, et al. Program synthesis with large language models. *arXiv preprint arXiv:2108.07732*, 2021b.
- Omer Bar-Tal, Hila Chefer, Omer Tov, Charles Herrmann, Roni Paiss, Shiran Zada, Ariel Ephrat, Junhwa Hur, Guanghui Liu, Amit Raj, et al. Lumiere: A space-time diffusion model for video generation. In *SIGGRAPH Asia 2024 Conference Papers*, pages 1–11, 2024.
- Tiwei Bie, Maosong Cao, Kun Chen, Lun Du, Mingliang Gong, Zhuochen Gong, Yanmei Gu, Jiaqi Hu, Zenan Huang, Zhenzhong Lan, Chengxi Li, Chongxuan Li, Jianguo Li, Zehuan Li, Huabin Liu, Lin Liu, Guoshan Lu, Xiaocheng Lu, Yuxin Ma, Jianfeng Tan, Lanning Wei, Ji-Rong Wen, Yipeng Xing, Xiaolu Zhang, Junbo Zhao, Da Zheng, Jun Zhou, Junlin Zhou, Zhanchao Zhou, Liwang Zhu, and Yihong Zhuang. LLaDA2.0: Scaling up diffusion language models to 100b. *arXiv preprint arXiv:2512.15745*, 2025.
- Andrew Campbell, Valentin De Bortoli, Jiaxin Shi, and Arnaud Doucet. Self-speculative masked diffusions. *arXiv preprint arXiv:2510.03929*, 2025.
- Charlie Chen, Sebastian Borgeaud, Geoffrey Irving, Jean-Baptiste Lespiau, Laurent Sifre, and John Jumper. Accelerating large language model decoding with speculative sampling. *arXiv preprint arXiv:2302.01318*, 2023.
- Mark Chen, Jerry Tworek, Heewoo Jun, Qiming Yuan, Henrique P. de Oliveira Pinto, Jared Kaplan, Harri Edwards, Yuri Burda, Nicholas Joseph, Greg Brockman, et al. Evaluating large language models trained on code. *arXiv preprint arXiv:2107.03374*, 2021.
- Zicong Cheng, Guo-Wei Yang, Jia Li, Zhijie Deng, Meng-Hao Guo, and Shi-Min Hu. DEER: Draft with diffusion, verify with autoregressive models. *arXiv preprint arXiv:2512.15176*, 2025.
- Karl Cobbe, Vineet Kosaraju, Mohammad Bavarian, Mark Chen, Heewoo Jun, Łukasz Kaiser, Matthias Plappert, Jerry Tworek, Jacob Hilton, Reiichiro Nakano, et al. Training verifiers to solve math word problems. *arXiv preprint arXiv:2110.14168*, 2021.
- OpenCompass Contributors. OpenCompass: A universal evaluation platform for foundation models. <https://github.com/open-compass/opencompass>, 2023.

- Yifeng Gao, Ziang Ji, Yuxuan Wang, Biqing Qi, Hanlin Xu, and Linfeng Zhang. Self speculative decoding for diffusion large language models. *arXiv preprint arXiv:2510.04147*, 2025.
- Itai Gat, Tal Remez, Neta Shaul, Felix Kreuk, Ricky TQ Chen, Gabriel Synnaeve, Yossi Adi, and Yaron Lipman. Discrete flow matching. *Advances in Neural Information Processing Systems (NeurIPS)*, 37:133345–133385, 2024.
- Dan Hendrycks, Collin Burns, Saurav Kadavath, Akul Arora, Steven Basart, Eric Tang, Dawn Song, and Jacob Steinhardt. Measuring mathematical problem solving with the MATH dataset. *arXiv preprint arXiv:2103.03874*, 2021.
- Jonathan Ho, Ajay Jain, and Pieter Abbeel. Denoising diffusion probabilistic models. In *Advances in Neural Information Processing Systems (NeurIPS)*, volume 33, pages 6840–6851, 2020.
- Jonathan Ho, Tim Salimans, Alexey Gritsenko, William Chan, Mohammad Norouzi, and David J. Fleet. Video diffusion models. *Advances in Neural Information Processing Systems (NeurIPS)*, 35: 8633–8646, 2022.
- Hugo Lavenant and Giacomo Zanella. Error bounds and optimal schedules for masked diffusions with factorized approximations. *arXiv preprint arXiv:2510.25544*, 2025.
- Yaniv Leviathan, Matan Kalman, and Yossi Matias. Fast inference from transformers via speculative decoding. In *Proceedings of the 40th International Conference on Machine Learning (ICML)*, pages 19274–19286. PMLR, 2023.
- Yaron Lipman, Ricky TQ Chen, Heli Ben-Hamu, Maximilian Nickel, and Matthew Le. Flow matching for generative modeling. In *The Eleventh International Conference on Learning Representations*, 2022.
- Anji Liu, Oliver Broadrick, Mathias Niepert, and Guy Van den Broeck. Discrete copula diffusion. In *The Thirteenth International Conference on Learning Representations*, 2024.
- Aaron Lou, Chenlin Meng, and Stefano Ermon. Discrete diffusion language modeling by estimating the ratios of the data distribution. In *International Conference on Learning Representations (ICLR)*, 2024.
- Nanye Ma, Mark Goldstein, Michael S. Albergo, Nicholas M. Boffi, Eric Vanden-Eijnden, and Saining Xie. SiT: Exploring flow and diffusion-based generative models with scalable interpolant transformers. In *European Conference on Computer Vision*, pages 23–40. Springer, 2024.
- Shen Nie, Fengqi Zhu, Zebin You, Xiaolu Zhang, Jingyang Ou, Jun Hu, Jun Zhou, et al. LLaDA: Large language diffusion models. *arXiv preprint arXiv:2502.09992*, 2025.
- William Peebles and Saining Xie. Scalable diffusion models with transformers. In *Proceedings of the IEEE/CVF International Conference on Computer Vision*, pages 4195–4205, 2023.
- Robin Rombach, Andreas Blattmann, Dominik Lorenz, Patrick Esser, and Björn Ommer. High-resolution image synthesis with latent diffusion models. In *Proceedings of the IEEE/CVF Conference on Computer Vision and Pattern Recognition*, pages 10684–10695, 2022.
- Subham Sekhar Sahoo, Marianne Arriola, Yair Schiff, Aaron Gokaslan, Edgar Marroquin, Justin T. Chiu, Alexander Rush, and Volodymyr Kuleshov. Simple and effective masked diffusion language models. In *Advances in Neural Information Processing Systems (NeurIPS)*, volume 37, 2024.
- Jiaming Song, Chenlin Meng, and Stefano Ermon. Denoising diffusion implicit models. In *International Conference on Learning Representations*, 2020a.
- Yang Song, Jascha Sohl-Dickstein, Diederik P. Kingma, Abhishek Kumar, Stefano Ermon, and Ben Poole. Score-based generative modeling through stochastic differential equations. In *International Conference on Learning Representations*, 2020b.
- Chen Wang, Hao-Yang Peng, Ying-Tian Liu, Jiatao Gu, and Shi-Min Hu. Diffusion models for 3d generation: A survey. *Computational Visual Media*, 11(1):1–28, 2025.

Rongyuan Wu, Tao Yang, Lingchen Sun, Zhengqiang Zhang, Shuai Li, and Lei Zhang. SeeSR: Towards semantics-aware real-world image super-resolution. In *Proceedings of the IEEE/CVF Conference on Computer Vision and Pattern Recognition*, pages 25456–25467, 2024.

Jiacheng Ye, Zhihui Xie, Lin Zheng, Jiahui Gao, Zirui Wu, Xin Jiang, Zhenguo Li, and Lingpeng Kong. Dream 7b: Diffusion large language models. *arXiv preprint arXiv:2508.15487*, 2025.

Jason Yim, Hannes Stärk, Gabriele Corso, Bowen Jing, Regina Barzilay, and Tommi S. Jaakkola. Diffusion models in protein structure and docking. *Wiley Interdisciplinary Reviews: Computational Molecular Science*, 14(2):e1711, 2024.

Jaehoon Yoo, Wonjung Kim, and Seunghoon Hong. ReDi: Rectified discrete flow. In *The Thirty-ninth Annual Conference on Neural Information Processing Systems*, 2025.

A Implementation Details of Compared Methods

We compare against three representative inference-time baselines, namely SSD [Gao et al., 2025], DCD [Liu et al., 2024], and DDOSP [Lavenant and Zanella, 2025]. For all comparing methods, we use the same LLaDA-Instruct checkpoint, prompt formatting, maximum generation length, and OpenCompass evaluation pipeline as in the main experiments. Unless otherwise stated, we keep the denoising step budget, block partition, temperature, classifier-free guidance scale, and re-masking rule identical to the LLaDA baseline, so that the differences come only from the inference strategy itself.

SSD. We implement SSD as a training-free decoding wrapper around the same LLaDA checkpoint. At each denoising step, the model first predicts all masked positions in parallel and uses the top-1 token at each masked position as the self-draft token. Candidate positions are selected within the current semi-autoregressive decoding block according to model confidence, and a greedy linear verification tree is constructed. All verification nodes are then packed into one batch and verified by the same LLaDA model. Therefore, SSD does not introduce an auxiliary draft model or any additional training. In the experiments, the same checkpoint is used as both the drafter and the verifier.

DCD. The original DCD formulation requires a diffusion model and an autoregressive copula model that share exactly the same tokenizer and token-to-id mapping. Because standard causal language models such as GPT-2 are not tokenizer-compatible with LLaDA, we implement a causalized DCD-like baseline by reusing the same LLaDA checkpoint with a causal attention bias as the copula model. At each denoising step, we compute diffusion logits l_{diff} and causalized copula logits l_{cop} , and form the proposal logits as

$$l_{\text{prop}} = l_{\text{cop}} + \alpha l_{\text{diff}},$$

where α controls the strength of the diffusion proposal and is set to 1.0 by default. For efficiency, we use the one-pass causal proposal mode in the main experiments, namely one causal forward pass per denoising step, while the sequential mode is reserved for additional analysis because it is substantially slower. Since LLaDA does not expose the same score/transition pair as the original Copula-Diffusion implementation, this baseline should be regarded as a DCD-style approximation rather than an exact reimplement of the original method.

DDOSP. DDOSP does not train a new model; instead, it replaces the handcrafted uniform unmasking schedule with a data-driven non-uniform schedule estimated from the denoiser. Specifically, we use training-set response sequences to estimate the information profile $f(i)$ under different numbers of revealed tokens, where the expectation is approximated by Monte Carlo masking and batched denoiser forward passes. The estimated profile is then smoothed and further corrected to be monotone before computing the incremental information gains $\Delta f(i)$. Based on these gains, we construct a K -step decoding schedule, cache the resulting schedule file, and reuse it during inference. During sampling, DDOSP only changes how many masked positions are released at each denoising round; the denoiser, token proposal rule, blockwise generation order, temperature, and re-masking strategy remain the same as in the LLaDA baseline. When no precomputed schedule is available, the implementation falls back to the uniform schedule.

B Implementation Details of Training

This section supplements the training details not explicitly reported in Section 4.1. In addition to the hardware and optimization settings described there, we report the released supplementary training runs and their usage in evaluation.

For the supplementary training setup, all runs were executed on 8 NVIDIA A100 80GB GPUs. The math training run used 18k examples for 1 epoch and took approximately 17.6 hours, corresponding to about 140.8 GPU-hours; the resulting model was used for evaluation on GSM8K and MATH. The code training run used 54k examples for 1 epoch and took approximately 52.8 hours, corresponding to about 422.4 GPU-hours; the resulting model was used for evaluation on HumanEval and MBPP. Summing these two runs gives an approximate total of 563.2 GPU-hours for the released supplementary training runs.

Additional implementation details are provided in Appendix A and Appendix C.

Algorithm 1 Position-Conditioned Training for FeF-DLLM

Require: Predictor p_θ , data distribution $q(X_0)$, response position set J_{resp}

Ensure: Trained predictor p_θ

1: **repeat**

2: Sample clean data $X_0 \sim q(X_0)$.

3: Sample diffusion time t .

4: Sample corrupted data $X_t \sim q(X_t | X_0)$.

5: Define the ordered prediction positions:

$$J_t = \{i \in J_{\text{resp}} : X_t^i \neq X_0^i\} = \{j_1, \dots, j_{L_t}\}, \quad j_1 < \dots < j_{L_t}, \quad L_t = |J_t|.$$

6: Initialize loss $\mathcal{L} \leftarrow 0$.

7: **for** $m = 1$ to L_t **do**

8: Construct the position-conditioned input $X^{(j_m)}$:

$$X^{(j_m),i} = \begin{cases} X_0^i, & i < j_m, \\ X_t^i, & i \geq j_m. \end{cases}$$

9: Compute the token-level cross-entropy loss:

$$\text{CE}_{j_m} = -\log p_\theta \left(X_0^{j_m} \mid X^{(j_m)}, t \right).$$

10: Accumulate loss:

$$\mathcal{L} \leftarrow \mathcal{L} + \text{CE}_{j_m}.$$

11: **end for**

12: Compute $\nabla_\theta \mathcal{L}$ and update θ with the optimizer.

13: **until** converged

14: **return** p_θ

C Algorithm

This section provides the detailed algorithms for FeF-DLLM. Algorithm 1 summarizes the position-conditioned training procedure. Algorithm 2 describes the full-sequence inference procedure, which combines speculative verification with low-confidence re-corruption.

Before presenting the inference algorithm, we define the residual distribution used when a draft token is rejected. For a target law $\pi_\theta^{j_m}$ and a draft law $\rho_\phi^{j_m}$ at position j_m , define

$$\pi_\theta^{j_m}(x) = \frac{\left[\pi_\theta^{j_m}(x) - \rho_\phi^{j_m}(x) \right]_+}{1 - \sum_{z \in \mathcal{V}} \min\{\pi_\theta^{j_m}(z), \rho_\phi^{j_m}(z)\}}, \quad (6)$$

where $[u]_+ = \max\{u, 0\}$. If the denominator is zero, the rejection event has probability zero, and the residual distribution is never sampled.

Algorithm 1 trains the model to predict each clean token from a position-conditioned input. For position j_m , tokens before j_m are replaced by their clean values from X_0 , while position j_m and the suffix remain in the corrupted state X_t . This construction matches the verification-time input used by the target model during left-to-right speculative verification, thereby aligning training with factorization-error-free inference.

Algorithm 2 describes the full-sequence inference procedure of FeF-DLLM. At each generation step, the method repeatedly applies speculative decoding over the unresolved prediction positions. The draft model M_ρ proposes up to k candidate clean tokens in the current speculative window, and the target model M_π verifies these candidates in a fixed left-to-right order using position-conditioned inputs. Accepted or corrected tokens are written back to the sequence and serve as clean prefix context for subsequent positions. If all candidates in the window are accepted, the whole window is committed; if one candidate is rejected, a corrected token is sampled from the residual distribution, the remaining draft tokens in the window are discarded, and a new speculative

Algorithm 2 Full-Sequence FeF-DLLM Decoding

Require: Initial corrupted sequence X_t , prediction positions J_{pred} , draft model M_ρ , target model M_π , window size k , number of steps N_{step} , resampling budget n_{rm}

Ensure: Final generated sequence \hat{X}_0

```
1: Initialize  $X \leftarrow X_t$ .
2: for  $s = 0$  to  $N_{\text{step}} - 1$  do
3:   Initialize  $\mathcal{C}^{(s)} \leftarrow \emptyset$ .
4:   while there exists an unresolved position in  $J_{\text{pred}}$  do
5:     Let  $J_t = \{j_1, \dots, j_{L_t}\} \subseteq J_{\text{pred}}$ , with  $j_1 < \dots < j_{L_t}$ , be the unresolved positions.
6:     Set  $b \leftarrow \min\{k, L_t\}$ .
7:     Compute draft laws  $\rho_\phi^{j_m}(\cdot) = \rho_\phi(X_0^{j_m} = \cdot \mid X, t)$  for  $m = 1, \dots, b$ .
8:     Sample draft tokens  $\tilde{X}_0^{j_m} \sim \rho_\phi^{j_m}(\cdot)$  for  $m = 1, \dots, b$ .
9:     Construct verification inputs  $X^{(j_m)}$  for  $m = 1, \dots, b$ ,
10:      each input uses the verified prefix and the draft prefix  $\tilde{X}_0^{j_1}, \dots, \tilde{X}_0^{j_{m-1}}$ .
11:     Compute target laws  $\pi_\theta^{j_m}(\cdot) = p_\theta(X_0^{j_m} = \cdot \mid X^{(j_m)}, t)$  for  $m = 1, \dots, b$ .
12:     for  $m = 1$  to  $b$  do
13:       Sample  $u_m \sim \text{Uniform}(0, 1)$ .
14:       if  $u_m \leq \min\{1, \pi_\theta^{j_m}(\tilde{X}_0^{j_m}) / \rho_\phi^{j_m}(\tilde{X}_0^{j_m})\}$  then
15:          $X^{j_m} \leftarrow \tilde{X}_0^{j_m}$ ,  $c_{j_m} \leftarrow \pi_\theta^{j_m}(\tilde{X}_0^{j_m})$ .
16:          $\mathcal{C}^{(s)} \leftarrow \mathcal{C}^{(s)} \cup \{(j_m, c_{j_m})\}$ .
17:       else
18:         Sample  $Z^{j_m} \sim \pi_\theta^{j_m}(\cdot)$  according to Eq. 6.
19:          $X^{j_m} \leftarrow Z^{j_m}$ ,  $c_{j_m} \leftarrow \pi_\theta^{j_m}(Z^{j_m})$ .
20:         Discard the remaining draft tokens and restart from the updated  $X$ .
21:          $\mathcal{C}^{(s)} \leftarrow \mathcal{C}^{(s)} \cup \{(j_m, c_{j_m})\}$ .
22:       break
23:     end if
24:   end for
25:   end while
26:    $\hat{X}_0^{(s)} \leftarrow X$ .
27:   if  $s < N_{\text{step}} - 1$  then
28:     Select  $R^{(s+1)} = \text{LowConf}_{n_{\text{rm}}}(\mathcal{C}^{(s)})$ .
29:     for each  $i \in R^{(s+1)}$  do
30:       Re-corrup  $X^i \sim q(X_t^i \mid \hat{X}_0^{(s), i})$ .
31:     end for
32:   end if
33: end for
34: return  $\hat{X}_0 = \hat{X}_0^{(N_{\text{step}}-1)}$ 
```

window starts from the updated sequence. After all prediction positions are resolved, the method selects low-confidence positions and re-corrups them through the D3PM forward kernel for the next generation step. This procedure preserves the accept-reject correction of speculative decoding while allowing low-confidence positions to be refined through repeated generation and re-corrupion steps.

D Theoretical Proofs

D.1 Proof of Lemma 1

Proof. For simplicity, we omit the timestep index in the probability notation. By the chain rule and the position-wise corruption assumption, we have

$$\begin{aligned}
p(X_0^i | X_t, X_0^{<i}) &= \frac{p(X_0^i | X_t)p(X_0^{<i} | X_t, X_0^i)}{p(X_0^{<i} | X_t)} \\
&= \frac{p(X_0^i | X_t)p(X_t | X_0^{<i}, X_0^i)p(X_0^{<i} | X_0^i)}{p(X_0^{<i} | X_t)p(X_t | X_0^i)} \\
&= \frac{p(X_0^i | X_t)p(X_t^{<i} | X_0^{<i})p(X_t^i | X_0^i)p(X_t^{>i} | X_0^i, X_0^{<i})p(X_0^{<i} | X_0^i)}{p(X_0^{<i} | X_t)p(X_t^i | X_0^i)p(X_t^{-i} | X_0^i)} \\
&= \frac{p(X_0^i | X_t)p(X_t^{<i} | X_0^{<i})p(X_t^{>i} | X_0^i, X_0^{<i})p(X_0^{<i} | X_0^i)}{p(X_0^{<i} | X_t)p(X_t^{-i} | X_0^i)} \\
&\propto \frac{p(X_0^i | X_t)p(X_t^{>i} | X_0^i, X_0^{<i})p(X_0^{<i} | X_0^i)}{p(X_t^{-i} | X_0^i)} \\
&\propto p(X_0^i | X_t) \frac{p(X_0^i | X_t^{>i}, X_0^{<i})}{p(X_0^i | X_t^{-i})}.
\end{aligned}$$

Moreover, since the forward corruption process factorizes across positions, $X_t^{<i}$ is generated only from $X_0^{<i}$. Hence, once $X_0^{<i}$ is conditioned on, $X_t^{<i}$ provides no additional information about X_0^i , which gives

$$p(X_0^i | X_t, X_0^{<i}) = p(X_0^i | X_t^{>i}, X_0^{<i}).$$

The first equality follows from the chain rule of conditional probabilities. The second equality expands $p(X_0^{<i} | X_t, X_0^i)$ by Bayes' rule. The third equality decomposes the corrupted sequence into prefix, current position, and suffix under the position-wise forward corruption process, with the suffix term understood as the marginal likelihood after integrating out $X_0^{>i}$. The fourth equality cancels the common factor $p(X_t^i | X_0^i)$. The first proportionality absorbs all terms independent of X_0^i into the normalization constant. The last proportionality rewrites the remaining likelihood ratio in terms of $p(X_0^i | X_t^{>i}, X_0^{<i})$ and $p(X_0^i | X_t^{-i})$. The proportionality is over X_0^i , with normalization over the vocabulary. \square

D.2 Proof of Theorem 1

Proof. Fix the corrupted state X_t and the ordered update set

$$J_t = \{j_1, \dots, j_{L_t}\}, \quad j_1 < \dots < j_{L_t}.$$

For each $j_m \in J_t$, the target model is instantiated as the oracle next-position law

$$\pi_\theta^{j_m}(x) = p^*(X_0^{j_m} = x | X_t^{\geq j_m}, X_0^{<j_m}, t), \quad m = 1, \dots, L_t.$$

Let $\rho_\phi^{j_m}$ denote the corresponding draft law.

We first verify the one-step correction. Condition on the already committed prefix before position j_m . Then both $\pi_\theta^{j_m}$ and $\rho_\phi^{j_m}$ are fixed categorical distributions on \mathcal{V} . A proposal $\tilde{X}_0^{j_m} \sim \rho_\phi^{j_m}$ is accepted with probability

$$a(\tilde{X}_0^{j_m}) = \min \left\{ 1, \frac{\pi_\theta^{j_m}(\tilde{X}_0^{j_m})}{\rho_\phi^{j_m}(\tilde{X}_0^{j_m})} \right\}.$$

We use the convention

$$\rho_\phi^{j_m}(x) \min \left\{ 1, \frac{\pi_\theta^{j_m}(x)}{\rho_\phi^{j_m}(x)} \right\} = \min \{ \pi_\theta^{j_m}(x), \rho_\phi^{j_m}(x) \},$$

which also covers the case $\rho_\phi^{j_m}(x) = 0$. If the proposal is rejected, the corrected token is sampled from

$$\pi_\theta^{j_m}(x) = \frac{\left[\pi_\theta^{j_m}(x) - \rho_\phi^{j_m}(x)\right]_+}{1 - \sum_{z \in \mathcal{V}} \min\{\pi_\theta^{j_m}(z), \rho_\phi^{j_m}(z)\}},$$

where $[u]_+ = \max\{u, 0\}$. If the denominator is zero, rejection occurs with probability zero, and the residual law is never used.

For any $x \in \mathcal{V}$, the probability that x is committed at position j_m is

$$\begin{aligned} \Pr(\hat{X}_0^{j_m} = x) &= \rho_\phi^{j_m}(x) \min\left\{1, \frac{\pi_\theta^{j_m}(x)}{\rho_\phi^{j_m}(x)}\right\} + \left(1 - \sum_{z \in \mathcal{V}} \min\{\pi_\theta^{j_m}(z), \rho_\phi^{j_m}(z)\}\right) \pi_\theta^{j_m}(x) \\ &= \min\{\pi_\theta^{j_m}(x), \rho_\phi^{j_m}(x)\} + \pi_\theta^{j_m}(x) - \min\{\pi_\theta^{j_m}(x), \rho_\phi^{j_m}(x)\} \\ &= \pi_\theta^{j_m}(x). \end{aligned}$$

Thus, given the committed prefix, the token committed by the speculative accept–reject step has law $\pi_\theta^{j_m}$.

Applying this argument sequentially along $j_1 < \dots < j_{L_t}$, for any $x_{J_t} = (x^{j_1}, \dots, x^{j_{L_t}}) \in \mathcal{V}^{L_t}$,

$$\begin{aligned} \Pr(\hat{X}_{0, J_t} = x_{J_t} \mid X_t, t) &= \prod_{m=1}^{L_t} \Pr(\hat{X}_0^{j_m} = x^{j_m} \mid X_t^{\geq j_m}, x_0^{< j_m}, t) \\ &= \prod_{m=1}^{L_t} \pi_\theta^{j_m}(x^{j_m}) \\ &= \prod_{m=1}^{L_t} p^*(X_0^{j_m} = x^{j_m} \mid X_t^{\geq j_m}, x_0^{< j_m}, t) \\ &= p^*(x_{J_t} \mid X_t, t). \end{aligned}$$

The last equality follows from the left-to-right factorization of the oracle joint law over the ordered set J_t . Hence the generated sequence has the desired oracle joint law. \square

D.3 Proof of Corollary 1

Proof. Fix a resampling pass $s \geq 1$. Let

$$R^{(s)} = \{r_1^{(s)}, \dots, r_{L_s}^{(s)}\}, \quad r_1^{(s)} < \dots < r_{L_s}^{(s)},$$

be the positions selected for resampling. We condition on the previous sequence $\hat{X}_0^{(s-1)}$ and on the selected set $R^{(s)}$. Under this conditioning, all positions outside $R^{(s)}$ are fixed, and the resampling pass only updates positions in $R^{(s)}$.

By the assumption of the corollary, the target model on $R^{(s)}$ is given by the oracle next-position law. Therefore, the same one-step accept–reject argument used in the proof of Theorem 1 implies that each committed token has the corresponding oracle law given the already committed prefix and the fixed outside positions. Applying the chain rule along the order

$$r_1^{(s)} < \dots < r_{L_s}^{(s)},$$

we obtain, for any $x_{R^{(s)}} \in \mathcal{V}^{L_s}$,

$$\begin{aligned} \Pr(\hat{X}_{0, R^{(s)}}^{(s)} = x_{R^{(s)}} \mid \hat{X}_0^{(s-1)}, R^{(s)}, t) \\ = p^*(x_{R^{(s)}} \mid \hat{X}_0^{(s-1)}, R^{(s)}, t). \end{aligned}$$

Thus, conditional on the resampling history and the selected resampling set, the regeneration step has the oracle joint law on the updated positions. \square

D.4 Proof of Theorem 2

Proof. In one speculative round, candidates are verified from left to right until the first rejection or until all k candidates are accepted. Let C_k denote the number of positions committed in this round. Since a rejected position is also committed after correction, the event $C_k > \ell$ is equivalent to accepting the first ℓ draft tokens.

Under the independent-acceptance approximation, each draft token is accepted with probability α . Hence, for $\ell = 0, \dots, k-1$,

$$\Pr(C_k > \ell) = \alpha^\ell.$$

By the tail-sum formula for nonnegative integer-valued random variables,

$$\begin{aligned} \mathbb{E}[C_k] &= \sum_{\ell=0}^{k-1} \Pr(C_k > \ell) \\ &= \sum_{\ell=0}^{k-1} \alpha^\ell. \end{aligned}$$

Evaluating the geometric series gives

$$\mathbb{E}[C_k] = \begin{cases} \frac{1 - \alpha^k}{1 - \alpha}, & 0 \leq \alpha < 1, \\ k, & \alpha = 1. \end{cases}$$

□

D.5 Proof of Corollary 2

Proof. A speculative round consists of one draft proposal pass and one target verification pass, with wall-clock costs c_ρ and c_π , respectively. Thus, its expected cost is $c_\rho + c_\pi$, and by Theorem 2 it commits $\mathbb{E}[C_k]$ positions in expectation.

The prefix-conditioned sequential target baseline commits one position per target pass, with cost c_π . Therefore, its expected cost for committing $\mathbb{E}[C_k]$ positions is $\mathbb{E}[C_k]c_\pi$. The idealized acceleration ratio is consequently

$$S = \frac{\mathbb{E}[C_k] c_\pi}{c_\rho + c_\pi}.$$

if $c_\rho \approx c_\pi$, then

$$S = \frac{\mathbb{E}[C_k]}{2}.$$

Substituting the expression for $\mathbb{E}[C_k]$ from Theorem 2 yields

$$S = \begin{cases} \frac{1 - \alpha^k}{2(1 - \alpha)}, & 0 \leq \alpha < 1, \\ \frac{k}{2}, & \alpha = 1. \end{cases}$$

□